HYDROLOGICAL PROCESSES
Hydrol. Process. **27**, 669–686 (2013)
Published online 17 October 2012 in Wiley Online Library
(wileyonlinelibrary.com) DOI: 10.1002/hyp.9552

Russian nesting dolls effect – Using wavelet analysis to reveal non-stationary and nested stationary signals in water yield from catchments on a northern forested landscape

Samson G. Mengistu,[1] Irena F. Creed,[2]* Reg J. Kulperger[3] and Christopher G. Quick[2]

[1] *Department of Earth Sciences, Western University, 1151 Richmond Street, London, Ontario, Canada, N6A 5B7*
[2] *Department of Biology, Western University, 1151 Richmond Street, London, Ontario, Canada, N6A 5B7*
[3] *Department of Statistics and Actuarial Sciences, Western University, 1151 Richmond Street, London, Ontario, Canada, N6A 5B7*

Abstract:

Determining catchment responses to climate signals gives insight into the potential effects of climate change. This study tested the hypothesis that a 28-year time series of water yields from four headwater catchments in the Turkey Lakes Watershed (TLW), Ontario contains signals of non-stationary climate change and naturally occurring stationary climate oscillations and that the effects of these signals are greater in catchments with lower rates of change in water loading and lower water storage capacity (small wetlands). Non-stationary trends explained 0%, 18%, 44%, and 52% of the variance in the water yields of the four catchments. Wavelet analysis using Morlet wavelets identified stationary responses at multiple temporal scales, increasing the amount of variance explained to 56%, 63%, 76%, and 81% when combining stationary and non-stationary models. The catchment with low water loading and low water storage was most sensitive to non-stationary and stationary signals, suggesting that these catchments act as sentinels to detect climatic signals. Wavelet coherence analysis revealed correlations between global climate oscillation indices and water yield. The Atlantic Multidecadal Oscillation (AMO) index was strongly correlated with both temperature and precipitation ($R^2 = 0.46$, $P < 0.001$ and R^2 of 0.34, $P < 0.001$, respectively). Temperature in the TLW increased by 0.067 °C per year from 1981 to 2008, but approximately 0.037 °C of this increase can be explained by the AMO index. While it is likely that anthropogenic climate change impacts water yields, it is important to account for multiple nested climate oscillations to avoid exaggerating its effects. Copyright © 2012 John Wiley & Sons, Ltd.

KEY WORDS anthropogenic climate change; catchment; climate; forest; non-stationary; stationary; time series analysis; water yield; wavelet analysis

Received 25 April 2012; Accepted 28 August 2012

INTRODUCTION

Climate effects on water resources continue to be a major agenda among hydrologists, ecologists, and policy makers. Catchments in various regions have been affected by non-stationary climate warming linked to anthropogenic activities (Arnell, 2004; Christensen *et al*., 2004; Chen *et al*., 2006; Pike *et al*., 2008; Zwiers *et al*., 2011). Meanwhile, catchments have also been affected by stationary climate patterns, driven by large-scale climatic oscillations caused by fluctuations in sea surface temperature or sea level pressure (Keener *et al*., 2010; Kahya, 2011; Niedzielski, 2011) [e.g. Multivariate El Niño Southern Oscillation (ENSO) Index (MEI), Atlantic Multidecadal Oscillation (AMO), Northern Atlantic Oscillation (NAO), and Pacific Decadal Oscillation (PDO)], although there is some evidence that these oscillations may not be strictly stationary [e.g. ENSO (Gaucherel, 2010)]. Observed temporal variability in water yields may reflect the combined effect of non-stationary climate trends and stationary climate oscillations with multiple periodicities (Zhou *et al*., 2008). There is a critical need to discriminate between non-stationary and stationary signals in changing water yields from these catchments.

Discriminating between non-stationary responses (deterministic responses where the statistical mean and variance change with time, predictably and unpredictably) and stationary responses (stochastic responses where the statistical mean and variance do not change with time) of catchments is an important step to better understand and predict the often different responses of catchments and their water yields to climate (Jones *et al*., 2012). Individual statistical analyses have emerged that enable us to resolve this complexity, including wavelet analysis where decomposition of a time series into a time-frequency space enables not only identification of the dominant wavelets (i.e. periodicities) in the time series, but also estimation of how the dominant wavelets change over time (Torrence and Compo, 1998; Santos and De Morais, 2008). Wavelet cross coherence analysis between the spectra of large-scale climatic oscillations and water yields can be used to identify specific climatic oscillations responsible for stationary signals in the water yield time series. Guiding principles are needed to combine these statistical analyses to discriminate non-stationary from stationary signals in catchment responses to climate.

*Correspondence to: Irena Creed, Department of Biology, Western University, London, ON N6A 5B7.
E-mail: icreed@uwo.ca

Small, headwater catchments have great potential to serve as sentinels for climate change because of their ability to respond rapidly to changing environmental conditions including freeze–thaw and flood–drought transitions and trends (Strand *et al.*, 2008). Headwater catchments typically have high topographic positions, collect precipitation from a relatively small area, and have thin soil layers for moisture storage, making their hydrologic regime more sensitive to climate-related changes in environmental conditions compared to the higher order catchments into which they drain (Feminella, 1996; Winter, 2000; Eimers *et al.*, 2004). Furthermore, headwater catchments contribute a large amount of water (Kirby, 1978; Haycock *et al.*, 1993) and constitute a large spatial extent (Meyer and Wallace, 2001; Sidle *et al.*, 2000; Bishop *et al.*, 2008) of larger catchments, and so have considerable influence on what may happen to higher order catchment water yields. In addition, these headwater catchments serve as sources of sediments, nutrients, and biota to downstream reaches of larger catchment systems (Rabeni and Wallace, 1998; Gomi *et al.*, 2002; Wipfli and Gregovich, 2002; Clarke *et al.*, 2008). Therefore, scientific investigations of the effects of climate-related environmental changes on water, sediment, and nutrient export would benefit from consideration of headwater catchments.

The purpose of this paper is to present an analytical framework for discriminating non-stationary and stationary signals in water yield responses of headwater catchments in a forested landscape where climatic variability is evident, but little is known about its effect on sustainability of water yields. The (null) hypothesis that climate has no significant effect on water yields was tested using a 28-year time series of water yields (the longest available within the region) from headwater catchments. If climate does have an effect, then a corollary to the hypothesis is that stationary signals are more important than non-stationary signals in water yields. Also, if climate does have an effect, then a corollary to the hypothesis is that sensitivity to these signals is greater in catchments that have lower rates of change in water loading and lower water storage capacity. By examining the ability of headwater catchments to respond to both directional climate change and non-directional naturally occurring climatic oscillations, it may be possible to infer what types of catchments may be the most sensitive sentinels of climate change and may see the most extreme impacts of continuing climate warming.

STUDY AREA

Located on the northern edge of the Great Lakes-St. Lawrence Forest Region in the Algoma Highlands of Central Ontario (Figure 1), the Turkey Lakes Watershed (TLW) is about 60 km north of Sault Ste. Marie (47°80'30"N, 84°82'50"W; Figure 2). In 1980, the TLW was established as a long-term experimental research station by Canadian federal government agencies to investigate the potential effects of acid rain and climate

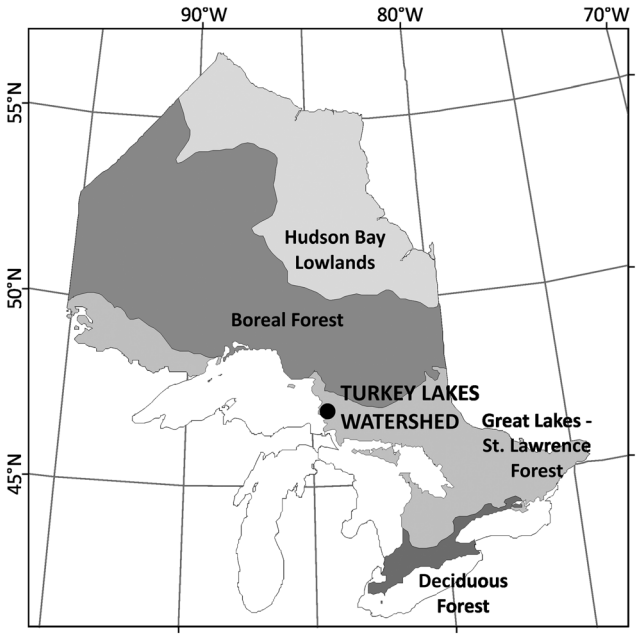

Figure 1. The forest eco-regions of Ontario

change on terrestrial and aquatic ecosystems (Jeffries *et al.*, 1988). Within the TLW, a series of headwater catchments representing the range of natural variation in geologic and geomorphic conditions have been continuously monitored for hydrology and biogeochemistry by Natural Resources Canada-Canadian Forest Service and Environment Canada scientists.

The TLW rests on Precambrian silicate greenstone formed from metamorphosed basalt, with small outcrops of felsic igneous rock (Giblin and Leahy, 1977). The overall relief is 400 m, from 644 m above sea level at the summit of Batchawana Mountain to 244 m above sea level at the outlet to the Batchawana River. Overlying the bedrock is a thin and discontinuous till, ranging in depth from <1 m at higher elevations to 1–2 m at lower elevations (Jeffries and Semkin, 1982), although till deposits up to 65 m occasionally occur in bedrock depressions (Elliot, 1985). The podzolic soils that have developed in the tills follow a generalized sequence of thin and undifferentiated near the ridge, gradually thickening, differentiating, and increasing in organic content on topographic benches and toward the stream (Nicolson, 1988). Highly humified organic deposits occur in wetlands (Canada Soil Survey Committee, 1978; Cowell and Wickware, 1983).

The watershed is covered by a northern-tolerant hardwood forest dominated by sugar maple (*Acer saccharum* Marsh.) (Wickware and Cowell, 1985). There have been no disturbances since the 1950s, except an experimental harvest in 1998 on a portion of the watershed. Average stand density (904 stems ha^{-1}), dominant height (20.5 m), diameter at breast height (15.3 cm), and basal area (25.1 m^2 ha^{-1}) are relatively uniform across the uplands, with stand density increasing and dominant height decreasing in the wetlands (Jeffries *et al.*, 1988). White pine (*Pinus strobes* L.), white spruce (*Picea glauca* Moench Voss.), ironwood (*Ostrya virginiana*

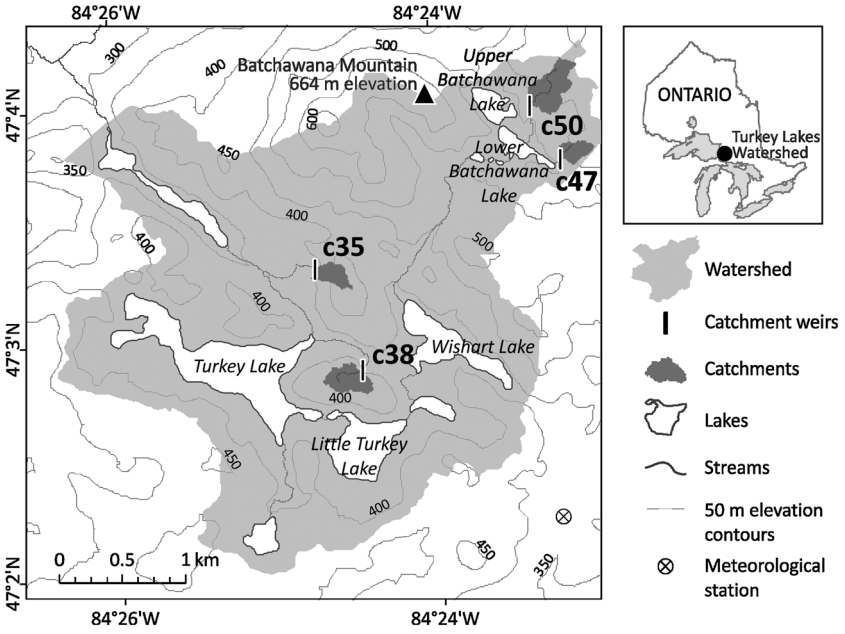

Figure 2. The Turkey Lakes Watershed

(Mill.) K. Koch), and yellow birch (*Betula alleghaniensis* Britton) comprise less than 10% of basal area in the uplands. The sparse understory of upland stands is dominated (95%) by saplings and seedlings of sugar maple as well as a variety of herbs and ferns. Wetland stands are mixtures of black ash (*Fraxinus nigra* Marsh.), eastern white cedar (*Thuja occidentalis* L.), red maple (*Acer rubrum* L.), balsam fir (*Abies balsamea* (L.) Mill.), yellow birch, and tamarack (*Larix laricina* (DuRoi) K. Koch.). The understory in the wetlands is composed of the seedlings and saplings of overstory trees and various herbs and ferns. There has been no to minimal natural or anthropogenic disturbance to the forest cover within these four catchments.

The watershed is influenced by a continental climate with average 28-year annual precipitation of 1200 mm and average annual temperature of 5 °C (Figure 3). Headwater catchments are influenced by a snowpack that persists from late November, early December through to late March, early April and peak flows that occur during snowmelt and again during autumn storms. Future climate scenarios for the area predict temperatures increasing by 1.0 to 3.0 °C by 2040 and 2.5 to 4.5 °C by 2070, and precipitation increasing by 0 to 10% by 2040 and 0 to 20% by 2070 (Price *et al.*, 2011). The four selected catchments, c35, c38, c47, and c50, exhibit a gradient in water loading in the form of rain and snow and in water storage in wetlands (percent wetlands by area) (Figure 4, Table I). Catchments c35 and c47 have low water storage (1.1% and 0.4%, respectively), while c38 and c50 contain high water storage (20.5% and 10.0%, respectively) (Creed *et al.*, 2008). All four catchments receive more precipitation than the site of the long-term meteorological station (Semkin *et al.*, 2001; unpublished data). Both c35 and c38 are at lower elevations and receive about 5% less precipitation than c47 and c50, but there is considerable inter-annual variation (Semkin *et al.*, 2001; unpublished data).

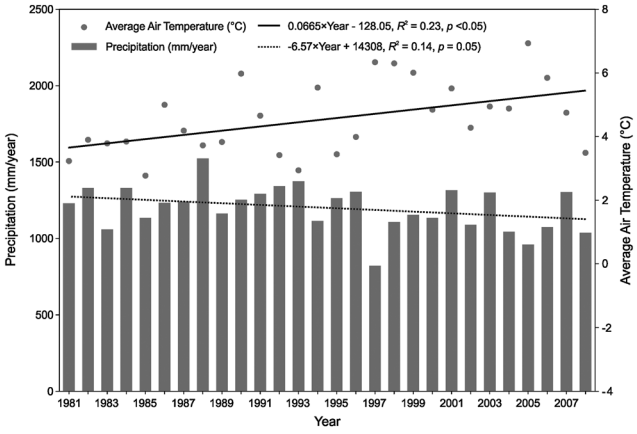

Figure 3. Annual hydroclimatic variation in the Turkey Lakes Watershed region

METHODS

Analytical framework

The analytical framework for analyzing non-stationary (linear trends) and stationary (non-linear oscillations) signals from the computed yearly water yield time series is presented in Figure 5.

Non-stationary linear trends

Annual data were used because daily, monthly, and seasonal water yield data were too variable and linear trends were not statistically significant (data not shown). Daily water yield data from four catchments (c35, c38, c47, and c50) in the TLW were summed to derive a yearly time series of water yield running from 1981 to 2008 water years (June–May, with the water year indicated as the calendar year in which the water year began). The computed yearly time series of water yields were analyzed for non-

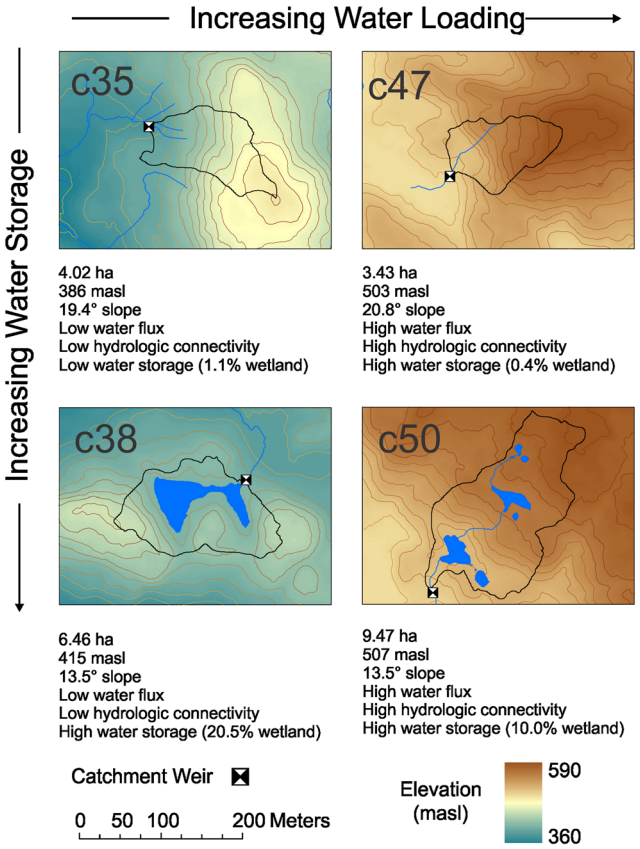

Figure 4. Topographic maps and descriptions of the four catchments selected from the Turkey Lakes Watershed for analysis

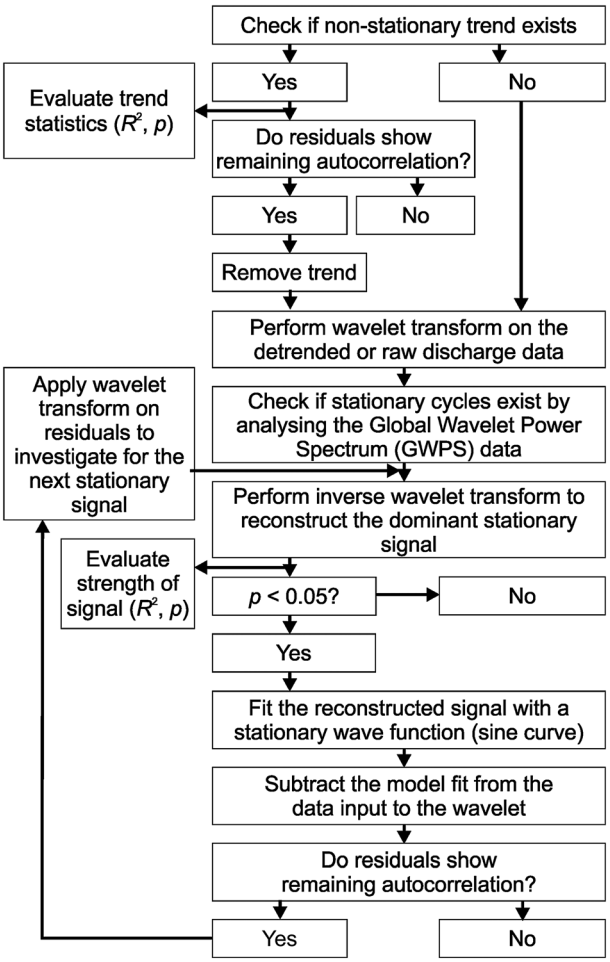

Figure 5. Flow chart summarizing the analytical steps

Table I. Characteristics of selected catchments in the Turkey Lakes Watershed

Characteristics	c35	c38	c47	c50
Size (ha)	4.02	6.46	3.43	9.47
% Wetland	1.06	20.54	0.36	10.03
Elevation of weir (masl)	386	415	503	507
Slope (degrees)	19.36	13.51	20.84	13.45

stationarity, which was then removed. The detrended portions were then further studied for the presence of multiple stationary signals using wavelet analysis.

Stationary non-linear oscillations

Following the method outlined in Torrence and Compo (1998), wavelet power spectrums of the detrended portion of the yearly water yield data were derived for the catchments under investigation. The spectrums were computed by convoluting each time series with a scaled and translated version of a transforming wavelet function, usually known as the 'mother wavelet.' Assuming an equal time interval of Δt in a time series X_n ($n = 0, 1, \ldots, N-1$), the corresponding wavelet function, $\psi_o(\eta)$ (η is a non-dimensional time parameter on which the function depends), must have a zero mean and be localized in time and frequency space (Farge, 1992). A Morlet wavelet was chosen due to its extensive applications in similar studies involving hydroclimatic time series analysis. In addition to its ability to represent the shape of hydrological signals very well (Kang and Lin, 2007), Morlet wavelets provide adequate time and superior frequency resolution compared to other wavelet types (Labat, 2005; Soniat *et al.*, 2006).

The Morlet wavelet is characterized by a Gaussian modulated plane wave:

$$\psi_o(\eta) = \pi^{-\frac{1}{4}} e^{i\omega_o \eta} e^{-\frac{\eta^2}{2}} \tag{1}$$

Where ω_o is the non-dimensional angular frequency, which by default is taken to be 6 to satisfy the admissibility condition (Farge, 1992).

The continuous wavelet transform of time series X_n, for each scale s at all n, with respect to the wavelet function $\psi_o(\eta)$, is mathematically represented as Equation (2).

$$W_n(s) = \frac{1}{N} \sum_{n'=0}^{N-1} x_{n'} \psi * \left[\frac{(\eta' - \eta)\Delta t}{s} \right] \tag{2}$$

Where $W_n(s)$ stands for wavelet transform coefficients, ψ for the normalized wavelet, (*) for the complex conjugate, s for wavelet scale, n for localized time index, and n' for translated time index.

The transformed signal, W_n (s), is a function of the wavelet scale and translation parameters found by conducting the convolution N (the number of data in the time series) times for each scale. Other than Equation (2), a faster way of performing such a transform is to simultaneously calculate all the N convolutions in a Fourier space using discrete Fourier transform of Xn Equation (3).

$$\widehat{x}_k = \frac{1}{N}\sum_{n=0}^{N-1} x_n e^{-2\pi ikn/N} \tag{3}$$

Where $k = 0 \ldots N$ is the frequency index. In the Fourier space, the wavelet transform Equation (2) can be expressed as Equation (4).

$$W_n(s) = \sum_{k=0}^{N-1} \widehat{x}_k \widehat{\psi} * (s\omega_k) e^{i\omega_k n\Delta t} \tag{4}$$

Where $\widehat{\psi}(s\omega)$ is Fourier transform of a function $\psi(t/s)$ and ω_k is an angular frequency defined as Equation (5).

$$\omega_k = \begin{cases} \dfrac{2\pi k}{N\Delta t} & if\ k \le \dfrac{N}{2} \\ -\dfrac{2\pi k}{N\Delta t} & if\ k > \dfrac{N}{2} \end{cases} \tag{5}$$

The wavelet power spectrum was calculated as the square of the absolute value of the wavelet transform, $|W_n\ (s)|^2$.

The global wavelet power spectrum (GWPS)-based analysis is considered a simple and robust technique for characterizing variability in time series (Santos and De Morais, 2008). Once the wavelet power spectrums were calculated, the GWPS values were computed by time averaging of wavelet spectrum values over all the local spectra. Generally, in wavelet-based time series analysis, it is believed that the GWPS values provide useful information in terms of assessing the scale(s) (or period (s)) contributing most to the spectral energy of the time series under investigation. Scales with large GWPS values were considered to contribute more spectral energy, while the contribution of small GWPS scales were assumed to be little or insignificant, The GWPS values were, therefore, used to identify scale(s) with high potential of periodic signals of stationary nature.

Inverse wavelet transfer of the forward wavelet transform Equation (2) above was employed to reconstruct signals based on the coefficients of scales identified to have dominant GWPS. The inverse wavelet function is mathematically represented as Equation (6).

$$x_n = \int_0^N \int_{S_1}^{S_k} W_n(s).\left[\frac{(\eta' - \eta)}{s}\right]\frac{dsdn}{s^2} \tag{6}$$

Maintaining the coefficients of the chosen scale(s) while replacing all scale coefficients by zero and performing backwards (inverse) wavelet transform on the result generated the signals characterizing the identified scale. When choosing two or more consecutive scales, the inverse transform function builds the reconstructed signal as the sum of wavelets of different scales, s, at localized time, n.

Autocorrelation tests were used to examine if there was temporal autocorrelation between yearly time series of water yield. The autocorrelation was tested using Matlab's *autocorr* function and the confidence bounds were found using (7).

$$+/- \frac{nSTDs}{sqrt(N)} \tag{7}$$

where *nSTD*s is the number of standard deviations used in determining significance, and N is the number of independent sample data points. Two standard deviations were used to approximate 95% significance.

Searching for multiple stationary signals

Stationary signals were extracted from the water yield data time series using a step-wise methodology involving multiple cycles. The first step of the first cycle used the wavelet power spectrum of the detrended water yield time series to identify the dominant periodicity in the detrended time series, which was followed by inverse wavelet transform to extract the signal of dominant periodicity corresponding to scale(s) of peak GWPS values. The extracted signal was then fitted with a periodic function to model and statistically analyse the stationarity of the extracted signal. The same steps were followed in the second cycle using the residual of the detrended data (detrended water yield minus modeled stationary signal from cycle 1) as the input to the wavelet analysis. In the following cycles, subsequent residuals (input data of the previous cycle minus modeled stationary signal in the same cycle) were similarily analyzed.

For each cycle, the following 'rules' were used to identify existing stationary signals: (1) A baseline of GWPS values was determined to select scales with the largest GWPS peaks above the set baseline, (2) Peak GWPS values were only considered for scales that were able to complete at least two full cycles in the available data (i.e. cycles with periods less than 14 years), (3) Subsequent peak GWPS values were analysed until their inclusion in the model was not significant, and (4) The same scale could not appear twice among signals. After selecting the stationary signals for each catchment, each signal was added to the model using forward step-wise regression against the raw water yield data, first with the non-stationary signal.

Wavelet cross coherence analysis

Wavelet cross coherence analysis was used to understand the dominant oscillations that have detectable periodic patterns in the yearly time series of water yield within the chosen catchments. Wavelet coherence (Torrence and

Webster, 1999; Grinsted *et al.*, 2004) of two time series X and Y, with wavelet transforms $W_n^X(s)$ and $W_n^Y(s)$, is defined as

$$R_n^2(s) = \frac{\left|S\left(s^{-1}W_n^{XY}(s)\right)\right|^2}{S\left(s^{-1}\left|W_n^X(s)\right|^2\right) \times S\left(s^{-1}\left|W_n^Y(s)\right|^2\right)} \quad (8)$$

where, S is a smoothing operator both in time and space that can be written as

$$S(W) = S_{\text{scale}}(S_{\text{time}}(W_n(s))) \quad (9)$$

where, S_{scale} denotes smoothing along the wavelet scale axis and S_{time} for the time axis.

Equation (8) closely resembles that of a traditional correlation coefficient. As a result, it is logical to consider wavelet coherence as a localized correlation coefficient in time frequency space (Grinsted *et al.*, 2004). The purpose of a smoothing operator is to help locate local maxima or high regions in a plot, such as the cross coherence plot. The operation involves a smoothing or bin parameter, which determines the number of nearby frequencies, relative to one of interest, averaged (in a manner depending on the smoothing filter) to obtain the estimate of the cross coherence at the given frequency, producing an estimator that achieves small mean square error, which simultaneously keeps the variance and bias small.

We used wavelet cross coherence to correlate annual average indices for water years that were computed from monthly average indices of large scale climatic oscillations with the detrended water yield of the chosen catchments at each period using a Matlab package from Grinsted *et al.* (2002). The MEI, AMO, NAO, PDO indices were selected due to their global influence (Figure 6, Table II). Wavelet transform plots map the correlations of wavelets of varying periods with the water yield time series, while wavelet cross coherence plots map the correlations of wavelets of varying periods with two different time series, the large scale climatic oscillations and the local water yield time series. In both cases, the cone of influence delimits regions of the plot that can be considered as part of the analysis. By analysing the plots, significant associations are indicated using warmer colours, and relationships with 95% confidence are circled. For wavelet cross coherence plots, arrows indicate the nature of the correlation: arrows to the left indicate negative correlations and arrows to the right indicate positive correlations (Grinsted *et al.*, 2004).

Climate drivers of yearly water yield time series

Correlations tests were performed among the global climate oscillations and between the global climate oscillations and local meteorological conditions. To examine correlations among the global climate oscillations, Pearson product moment correlation tests were performed between each of the four climate indices selected. Significant correlations were not expected if the global climate oscillations were significantly correlated for a short period (e.g. if they were only strongly correlated for 5 years in a 28-year data series). Therefore, significant correlations among the global climate oscillations occurred only if they existed for nearly the entire time series.

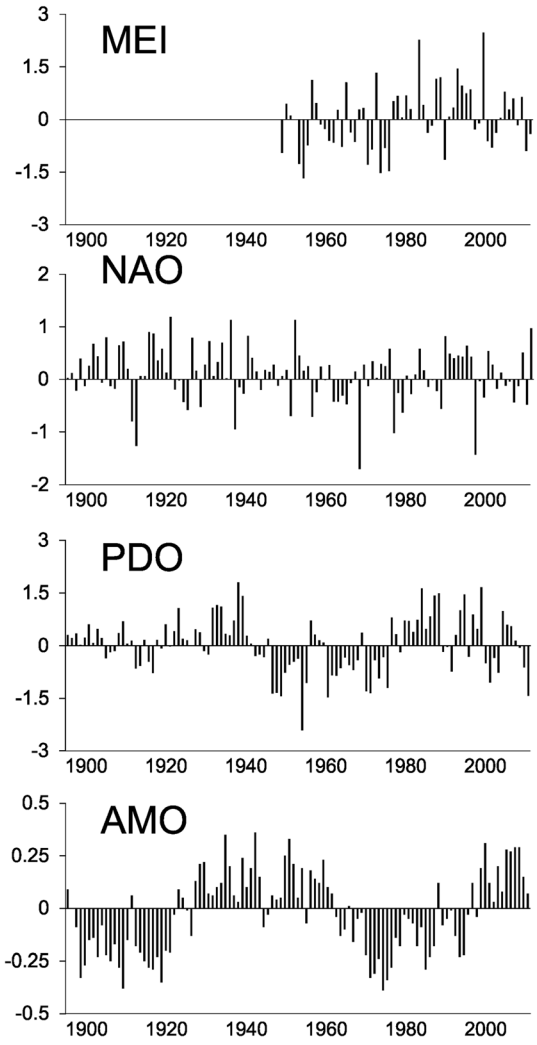

Figure 6. Time series of the Multivariate El Niño Southern Oscillation (ENSO) Index (MEI), Atlantic Multidecadal Oscillation (AMO), Northern Atlantic Oscillation (NAO), and Pacific Decadal Oscillation (PDO) indices

To examine correlations between the global climate oscillations and local meteorological conditions, we sought the longest possible meteorlogical records located near the four catchments in the TLW: the National Climatic Data Center's Global Historical Climatology Network v2 (GHCN-Monthly) station at Sault Ste. Marie, Michigan (Station identifier 42572734000, with a record from 1889 to 2011) and Environment Canada's station at Sault Ste. Marie, Ontario (Station identifier 71260, with a record from 1962 to 2011). Furthermore, data from the Michigan station were split into two periods (1901–1963 and 1964–2010) to compare the relationship between AMO and temperature/precipitation during distinct cycles of the estimated 60- to 90-year AMO global climate oscillation.

RESULTS

There were significant non-stationary signals in water yields. Catchments showed significant negative linear

Table II. Large-scale climatic oscillations used for cross-coherence analysis

Indices (data source)	Periodicity	Climatic influence
Multivariate El Nino Southern Oscillation (ENSO) Index (MEI) (NOAA – ESRL, 2012a)	The periodicity of strong ENSO events is approximately 2 to 7 years (Huggett, 1997).	A positive MEI index (an ENSO episode) is associated with warmer than normal autumn to spring temperatures at the study site (Shabbar and Khandekar, 1996, Shabbar and Bonsal, 2004).
Northern Atlantic Oscillation (NAO) (NCAR, 2012)	There is no statistically significant periodicity, although there is some evidence of a 7 to 9 year and approximately 20-year periodicities (Burroughs, 2005).	A positive NAO is associated with colder than normal winters at the study site (Bonsal *et al.*, 2001).
Pacific Decadal Oscillation (PDO) (JISAO, 2012)	PDO tends to occur with a periodicity of around 20 to 30 years (Burn, 2008; Mantua and Hare, 2002; Minobe, 1997)	A positive PDO is associated with warmer and drier winters, while negative phases are associated with cooler and wetter winters at the study site (Burn, 2008).
Atlantic Multidecadal Oscillation (AMO) (NOAA – ESRL, 2012b)	AMO is characterized by a 60- to 90-year oscillation (Knudsen *et al.*, 2011).	A positive AMO anomaly is associated with warmer winters and lower rainfall at the study site (Knight *et al.*, 2006).

trends in the yearly water yield time series over the past 28 years (Figure 7). The rate of decline in water yield was highest (−14.6 mm/year) in the catchment with lower water loading and lower water storage capacity (c35) ($R^2 = 0.52$, $p < 0.001$) and nearly as high (−13.0 mm/year) in the catchment with similar water loading but higher water storage capacity (c38) ($R^2 = 0.44$, $p < 0.001$). In contrast, the rate of decline in water yields was lowest (no significant signal) in the catchment with higher water loading and lower water storage capacity (c47) ($R^2 = 0.04$, $p = 0.306$), and higher (−8.9 mm/year) in the catchment with higher water loading and higher water storage capacity (c50,) ($R^2 = 0.18$, $p < 0.05$), but not as high as the lower water loading catchments. Non-stationary signals were influenced more by water loading than by water storage capacity.

There were also significant stationary signals in water yields. The sequence of steps for detecting significant stationary signals is illustrated for c35 in Figures 8, 9, and 10. After removing the linear trend in the water yield data of each catchment (Figures 8A–10A), wavelet transforms (Figures 8B–10B) and peak analysis (Figures 8C–10C) revealed periods that explained significant amounts of variance in the detrended water yield. Sine curves were modeled to the detrended water yield data (Figures 8D–10D), and while the autocorrelation function values from the residuals were all between 0.5 and −0.5 (Figures 8E–10E), indicating no significant autocorrelation with 95% confidence, the residuals suggested that periodic characteristics remained, so additional steps were undertaken until fitted scales were no longer statistically significant.

Each of the four catchments showed three significant stationary signals with the same periods (i.e. 2 to 2.83 years, 3.36 to 4.76, and 6.73 to 9.51 years), except for c50, which had a stationary signal of 5.66 to 8 years instead of 6.73 to 9.51 years (Tables III and IV). The relative dominance of these three periods varied among the catchments. The two catchments with lower water storage capacity (c35, c47) showed the same sequence of 6.73 to 9.51 detected first, followed by 2 to 2.83, and then 3.36 to 4.76 years. In contrast, the two catchments with higher water storage capacity (c38, c50) showed a different sequence from both the lower water storage capacity catchments and each other. The 2 to 2.83-year signal was detected first in both c38 and c50, but the sequence was 6.73 to 9.51 then 3.36 to 4.76 in c38 and the opposite in c50 (Table III). Signals with shorter

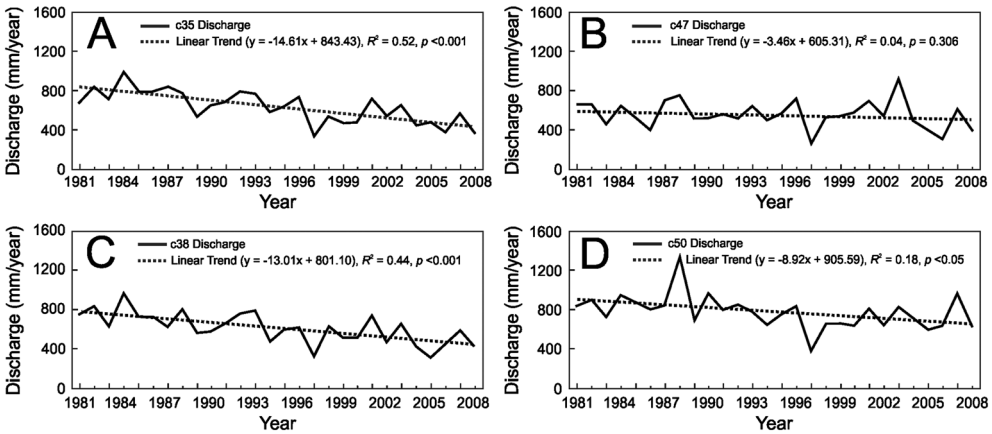

Figure 7. Non-stationary trends in water yield for (A) c35, (B) c47, (C) c38, and (D) c50

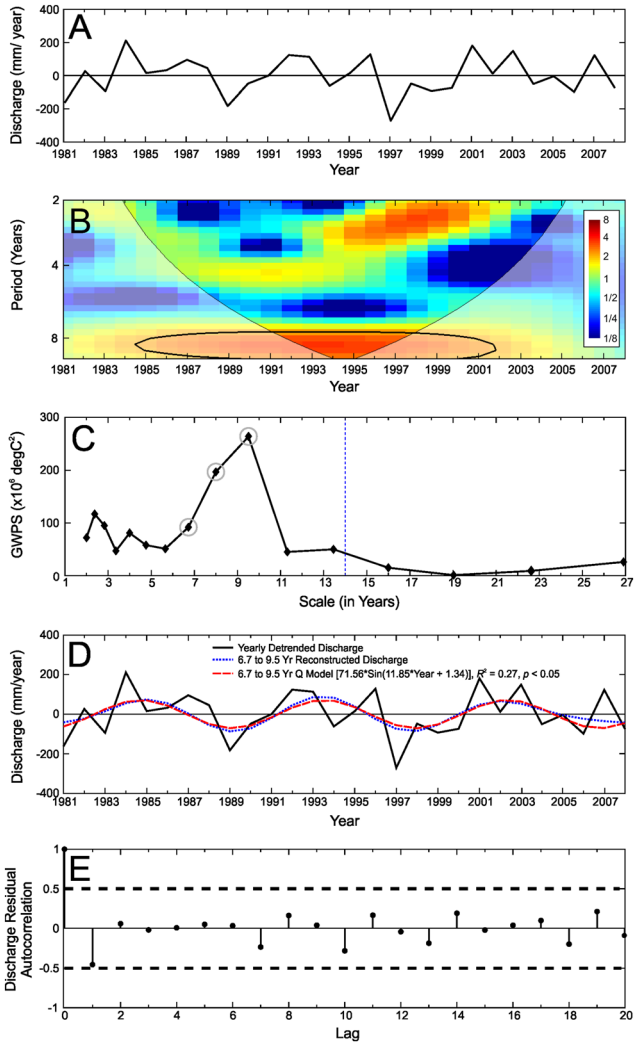

Figure 8. Stationary trend analysis for the first signal in c35: (A) c35 yearly detrended water yield data, (B) wavelet transform (from Equation 6) of c35 water yield data [strong and weak contributions to the power spectrum are indicated by warm (red) colours and cold (blue) colours, respectively, on a logarithmic scale; the thin solid line represents the cone of influence, the thick solid lines show the 95% significance level], (C) scale selection based on Global Wavelet Power Spectrum [the dotted line at 14 years indicates the cutoff for selecting periods of signals (half the 28-year time series)], (D) modeling the sine function to the detrended water yield data, and (E) Auto-correlation function analysis for the residuals between the observed and modeled water yield. Subsequent steps repeated the same process until fitting scales were no longer statistically significant

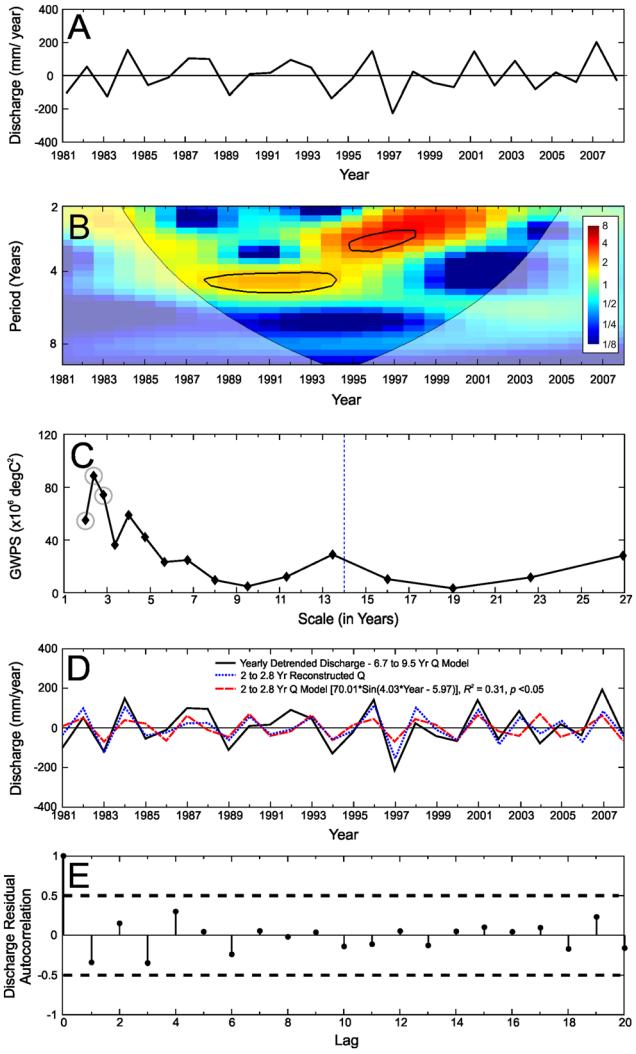

Figure 9. Stationary trend analysis for the second signal in c35: (A) c35 yearly detrended water yield data, (B) wavelet transform of c35 water yield data, (C) scale selection based on Global Wavelet Power Spectrum, (D) modeling the sine function to the detrended water yield data, and (E) Auto-correlation function analysis for the residuals between the observed and modeled water yield

periods dominated the detrended water yield time series in catchments with high water storage capacity, while the signals with longer periods dominated the time series in the catchments with small wetlands.

The combination of non-stationary and stationary signals explained the majority of variation in water yields for each of the four catchments: 81% (c35), 76% (c38), 56% (c47), and 63% (c50) (Figure 11, Table IV). For catchments with lower water loading (c35, c38), the non-stationary signal was higher than the combination of stationary signals. For c35 (low water storage capacity), the non-stationary signal explained 52% of the temporal variation in water yields, while the stationary signals together explained an additional 29%. For c38 (high water storage capacity), the relative importance of the two signals shifted slightly, with the non-stationary signal explaining 44% of the temporal variation in water yields, while the stationary signals together explained an additional 32%. In contrast, for catchments with higher water loading (c47, c50), the non-stationary signals were lower than the combination of stationary signals. For c47 (low water storage capacity), the non-stationary signal explained no variation in water yields, while the stationary signals explained 56% of the variation in water yields. Similarly, for c50 (high water storage capacity), the non-stationary signal explained 18% of the variation in water yields, while the stationary signals explained an additional 45% of the variation in water yields (Table IV). The modeled water yields represented the observed water yields in each of the four catchments; however, the modeled water yield sometimes failed to capture peak water yield, particularly in the catchments with high water loading, c47 (e.g. 2003 peak) and c50 (e.g. 1997 peak) (Figure 10).

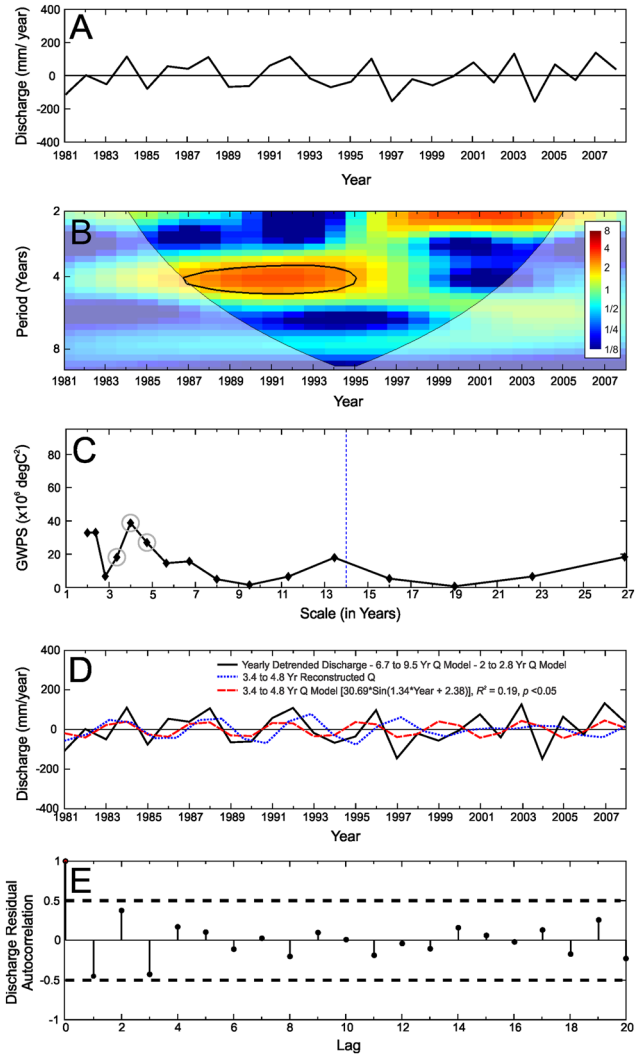

Figure 10. Stationary trend analysis for the third signal in c35: (A) yearly detrended water yield data, (B) wavelet transform of c35 water yield data, (C) scale selection based on Global Wavelet Power Spectrum, (D) modeling the sine function to the detrended water yield data, and (E) Auto-correlation function analysis for the residuals between the observed and modeled water yield

The wavelet cross coherence plots revealed complex interactions between water yield and global climate oscillations (Figures 12–15). For each of the four catchments, there were significant correlations between each of global climate oscillations and water yields: (1) MEI was highly correlated to water yields at periods of 2 to 3.5 years, particularly in the 1990s (coincident with PDO), with higher MEI resulting in lower water yields (Figure 12A–15A); (2) AMO was correlated to water yields at periods of 3 to 5 years, although the correlations were stronger at the beginning of the time series compared to the end of the time series, with higher AMO resulting in lower water yields (Figure 12B–15B); (3) NAO was correlated to water yields at periods of 3 to 4.5 years, particularly in the first half of the time series; however, the nature of the correlation was unclear (arrows in different directions) (Figures 12C–15C); and (4) PDO was highly correlated to periods of 2 to 3.5 years, particularly during the 5-year window from 1998 to 2003, with higher PDO resulting in lower water yields (Figures 12D–15D).

There were significant interactions among major climatic oscillation indices (i.e. MEI, AMO, NAO, and PDO) (Table V). The Pearson product moment correlation between the annual average values of the climate oscillations revealed significant correlations between the MEI and PDO ($p < 0.001$) and the NAO and PDO ($p < 0.05$). Of the 12 stationary signals observed in water yield data, six were significantly correlated with a climatic index (Table VI). MEI was the index most often strongly correlated with water yield (seven times total with four correlations being significant).

Comparing meteorological records at nearby stations with the major climatic oscillation indices, only the AMO index was significantly linked to temperature and precipitation at the TLW meteorological station. Temperature and the AMO index were positively linked from 1981 to 2008 ($R^2 = 0.46$, $p < 0.001$). This positive relationship was confirmed using the longer records of the Sault Ste. Marie, Michigan station (1889–2010, $R^2 = 0.19$, $p < 0.001$) and the Sault Ste. Marie, Ontario station (1962–2010; $R^2 = 0.35$, $p < 0.001$). Precipitation and the AMO index were negatively linked at the TLW station ($R^2 = 0.34$, $p < 0.001$), though no significant relationships were observed with data from the Michigan or Ontario stations.

Splitting the Michigan meteorological data according to distinct AMO cycles (1901–1963 and 1964–2010) revealed a change in the relationships. Split temperature records confirmed consistent positive relationships between the AMO index and temperature (Figure 16A), but split precipitation records indicated that from 1901 to 1963, AMO was significantly positively correlated to precipitation ($R^2 = 0.16$, $p < 0.05$), but during 1964 to 2010, AMO was negatively correlated with precipitation ($R^2 = 0.08$, $p < 0.05$) (Figure 16B). Looking at the complete AMO cycle from 1901 to 1963 *versus* temperature (Figure 16A), the minimum AMO value of −0.39 corresponds to an interpolated temperature value of 3.81 °C and the maximum AMO value of 0.36 corresponds to a temperature value of 4.96 °C. The difference of 1.15 °C over 31 years (half the AMO period) indicates that 0.037 °C per year in climate warming can be explained by a shift from a low point in the AMO cycle to a high point, about 55% of the observed 0.067 °C per year observed in the TLW (Figure 3).

DISCUSSION

This paper examined the effects of changing climatic conditions on water yields from headwater catchments on a natural (undisturbed) northern forested landscape. Northern latitudes are expected to see substantial environmental changes based on projected climate change scenarios (Carey *et al.*, 2010). We were interested to see if and how these effects are already being manifested. By focusing on headwater catchments on natural landscapes, we examined the hydrological systems that are most sensitive and that have the potential to serve as early warning sentinels of climate change effects to more

Table III. Global wavelet power spectrum (GWPS) values of water yield generated from Equation 6 in catchments c35 (A), c38 (B), c47 (C), and c50 (D). The detrended water yield was used to generate the first signal from the wavelet transform. Water yield used for subsequent signals is the difference between water yield from the previous step and modeled water yield at the step of investigation. The highlighted values indicate the peak GWPS values selected as the stationary signal in each step. See Figures 5–7 for sample peak selection

A – c35

Level	Period (Years)	Stationary Signal 1	Stationary Signal 2	Stationary Signal 3	Stationary Signal 4
1	2	72,742,838.99	52,559,388.15	32,799,491.02	27,446,013.24
2	2.38	117,046,896.11	86,142,685.27	33,099,842.66	27,794,912.71
3	2.83	95,367,771.17	71,792,782.62	6,696,663.58	4,232,105.67
4	3.36	47,741,733.74	33,848,471.69	18,165,496.28	2,583,822.86
5	4	81,074,024.78	56,401,908.76	38,739,832.75	10,806,888.73
6	4.76	58,234,715.87	39,741,839.00	26,980,918.02	17,925,972.20
7	5.66	51,335,670.69	20,873,913.33	14,592,670.07	10,317,740.44
8	6.73	92,205,150.66	22,340,644.25	15,694,400.58	11,632,192.79
9	8	197,102,724.56	7,197,672.74	4,958,396.31	3,739,473.63
10	9.51	264,112,013.58	2,417,747.20	1,526,098.69	1,211,442.02
11	11.31	45,201,766.78	9,685,764.83	6,538,213.21	5,017,783.08
12	13.45	50,842,798.77	26,525,867.07	17,936,846.25	13,754,007.79
13	16	15,053,551.08	7,880,583.29	5,330,643.82	4,090,358.01
14	19.03	1,053,004.09	969,869.79	691,324.14	586,426.30
15	22.63	9,521,102.60	9,229,953.56	6,601,178.77	5,632,752.84
16	26.91	26,474,669.50	25,665,094.95	18,355,442.43	15,662,607.47

B – c38

Level	Period (Years)	Stationary Signal 1	Stationary Signal 2	Stationary Signal 3	Stationary Signal 4
1	2	106,001,656.86	65,500,872.94	48,315,829.46	37,976,716.25
2	2.38	176,776,699.36	73,227,373.56	56,593,670.61	41,443,685.28
3	2.83	163,347,155.50	29,417,499.54	24,119,780.39	11,899,508.67
4	3.36	94,230,821.75	53,245,045.28	40,833,464.41	7,754,080.30
5	4	94,604,196.33	73,783,452.65	46,187,212.25	10,742,035.21
6	4.76	72,194,221.50	55,545,861.64	29,425,631.37	15,231,178.55
7	5.66	63,011,768.80	51,616,100.99	17,665,216.18	9,873,949.32
8	6.73	121,492,134.14	95,498,143.63	25,383,305.84	15,629,556.19
9	8	135,031,783.10	99,286,457.90	8,232,465.30	5,436,313.37
10	9.51	153,895,573.39	110,475,543.03	1,763,117.56	1,617,943.44
11	11.31	18,359,957.45	12,445,607.56	2,421,615.86	1,806,002.61
12	13.45	7,256,840.78	3,152,322.63	6,311,266.97	4,617,283.87
13	16	2,184,458.85	974,902.91	1,906,954.17	1,391,336.79
14	19.03	967,872.18	978,304.53	871,358.10	562,080.93
15	22.63	9,648,040.81	9,846,927.33	8,690,551.80	5,593,546.42
16	26.91	26,827,644.36	27,380,675.06	24,165,220.47	15,553,590.24

regional catchments, including those that provide water supplies to downstream communities.

Climate change has effects on water yields

The analytical framework outlined in this paper (Figure 5) enabled the detection of climate signals in the water yields of four catchments in the TLW. The framework detected non-stationary linear trends, then after removing these trends, detected stationary non-linear cycles caused by climate oscillations. Without applying this framework, these climate signals would not have been identified, discriminated, nor quantified from the original time series of water yields.

Climate had a substantial non-stationary effect on water yields. A shift to warmer and drier conditions resulted in a linear decline in water yields that ranged from 0% (c47) to 52% (c35). This decline of yearly water yield may be related to a unidirectional change towards warmer and drier conditions over the past 28 years. However, climate also had a substantial stationary effect on water yields. Multiple scales of nested periodic cycles were detected in the water yield data, explaining variation in addition to the non-stationary trends that ranged from c35 (29%) to c47 (56%). The three periodic cycles, which occurred from 2 to 2.83 years, 3.36 to 4.76 years, 6.73 to 9.51 years, were found in all catchments, except for c50, where the longest periodic trend was 5.66 to 8.00 rather than 6.73 to 9.51. A comparison of the periods from the wavelet analysis (Figures 8–10, Table III) and the wavelet cross coherence analysis (Figures 12–15) suggests that the 2 to 2.83-year signal was influenced by the MEI and PDO; the 3.36 to 4.76-year signal was influenced by the AMO; and the 6.73 to 9.51-year signal was influenced partially by the NAO, though it was only strongly correlated to water yields for the higher water loading

Table III. (*Continued*)

C – c47

Level	Period (Years)	Stationary Signal 1	Stationary Signal 2	Stationary Signal 3	Stationary Signal 4
1	2	157,378,239.90	130,985,771.78	103,534,002.71	64,157,739.24
2	2.38	238,019,826.75	197,689,749.78	93,014,746.78	62,664,581.73
3	2.83	236,765,895.02	197,011,424.17	51,846,652.20	18,944,890.45
4	3.36	193,389,465.55	160,463,022.85	105,140,813.67	10,874,058.26
5	4	197,170,649.88	162,055,920.48	129,181,221.50	4,760,670.53
6	4.76	66,672,825.22	44,838,963.34	37,913,995.80	9,819,489.91
7	5.66	161,946,538.57	25,973,696.09	23,481,299.18	18,331,077.33
8	6.73	423,081,833.54	45,421,536.92	39,531,938.84	28,953,133.67
9	8	207,480,165.06	81,090,984.09	62,461,506.46	46,627,686.57
10	9.51	135,564,307.08	110,929,919.49	83,073,858.35	62,119,444.50
11	11.31	92,175,460.96	79,159,848.22	56,239,813.54	39,268,364.16
12	13.45	220,101,911.49	190,401,174.75	134,047,200.73	92,409,319.83
13	16	65,257,544.17	56,448,360.73	39,748,733.61	27,397,450.38
14	19.03	5,489,763.99	4,678,540.27	3,451,728.12	2,293,780.81
15	22.63	50,655,197.95	43,105,691.36	31,948,504.04	21,155,114.85
16	26.91	140,853,402.31	119,861,011.50	88,836,994.23	58,824,563.32

D – c50

Level	Period (Years)	Stationary Signal 1	Stationary Signal 2	Stationary Signal 3	Stationary Signal 4
1	2	347,530,485.98	237,768,185.59	179,026,156.86	153,497,536.92
2	2.38	392,660,317.07	129,919,942.14	91,315,689.24	78,293,766.94
3	2.83	437,477,169.71	60,073,959.61	21,922,598.28	18,783,311.38
4	3.36	300,915,850.89	178,837,671.90	16,154,965.00	13,633,355.93
5	4	323,010,771.88	248,900,020.12	11,055,093.84	7,544,101.66
6	4.76	110,746,232.35	78,420,959.73	18,871,232.68	7,017,206.14
7	5.66	100,538,905.89	81,222,487.51	50,338,414.75	2,258,900.74
8	6.73	176,988,435.47	165,444,943.04	113,468,010.56	623,426.91
9	8	67,184,433.77	65,711,576.85	43,635,232.31	2,342,173.59
10	9.51	53,122,685.79	46,737,650.63	30,147,648.03	14,541,131.78
11	11.31	309,051,767.56	215,367,355.62	153,370,958.01	122,549,864.32
12	13.45	853,003,199.84	591,660,421.54	422,246,007.10	340,091,344.81
13	16	253,770,934.12	176,267,394.30	125,815,125.46	101,392,846.08
14	19.03	38,213,673.55	31,454,954.80	22,839,047.47	19,529,737.85
15	22.63	368,033,540.57	305,451,014.96	221,951,169.09	190,267,619.61
16	26.91	1,023,365,499.83	849,346,601.61	617,164,331.78	529,064,070.81

catchments, c35 and c38. A 28-year dataset is particularly short for wavelet analysis. It is likely that signals with longer periods are also present, but they could not be detected with the data available.

Climate change results in differential responses among catchments

There were substantial differences in the non-stationary rate of decline and a marginal difference in stationary oscillations in water yield signals among the catchments, despite their close proximity (Figure 7, Table IV). Catchments with lower water loading were more sensitive to the non-stationary climate signals (Table IV), showing declines in water yields of −14.6 mm/year (c35) and −13.0 mm/year (c38). Our findings suggest that there is a higher rate of change in net water loading (precipitation *minus* evapotranspiration and sublimation) on sites that experience less overall water loading, leading to a higher rate of change in catchment water yields at low water loading sites compared to higher water loading sites.

Catchments with wetlands formed by topographic depressions and/or flats store water (Lindsay *et al*., 2004; Creed *et al*., 2003; 2008). Catchments with higher water storage capacity buffered the effects of climate warming. The declines in water yield in catchments with lower water loading (c35 and c38) were of a greater magnitude than in those with higher water loading (c47 and c50). For the catchments with lower water loading (c35, c38), a lower water storage capacity increased the amount of variation explained in water yields attributed to non-stationary signals (52% for c35 *vs* 44% for c38), but increased the amount of model variation attributed to stationary signals (an additional 29% for c35 *vs* 32% for c38). For the catchments with higher water loading (c47, c50), a lower water storage decreased the amount of variation explained in water yields attributed to non-stationary signals (0% for c47 *vs* 18% for c50), and increased the amount of model variation attributed to stationary signals (an additional 56% for c47 and 45% for c50). Higher water storage capacity appeared to reduce the effects of shorter periods on discharge, perhaps

Table IV. Results of forward step-wise regressions of non-stationary (linear) and stationary (periodic) trends in raw water yield data from catchments c35, c38, c47, and c50 in the Turkey Lakes Watershed. Data reported are R^2 values (NS indicates not significant; * indicates $p < 0.05$; ** indicates $p < 0.01$; and *** indicates $p < 0.001$)

	c35	c38	c47	c50
Slope of Linear Trend (mm/year)	−14.8	−13.0	NS	−8.9
Individual R^2 values				
Linear Trend *versus* Raw Q	0.52***	0.44***	NS[a]	0.18*
Signal 1 *versus* Raw Q – Linear trend	0.27**	0.26**	0.19*	0.26**
Signal 2 *versus* Raw Q – Linear trend, Signal 1	0.31**	0.26**	0.23**	0.28**
Signal 3 *versus* Raw Q – Linear trend, Signal 1, 2	0.19*	0.26**	0.32**	0.15*
Signal 4 *versus* Raw Q – Linear trend, Signal 1, 2, 3	NS	NS	NS	-[b]
Cumulative R^2 values *versus Raw* Water yield				
Linear trend	0.52***	0.44***	NS[a]	0.18*
Linear trend + Signal 1	0.65***	0.59***	0.19 *	0.39***
Linear trend + Signal 1 + Signal 2	0.76***	0.68***	0.38***	0.56***
Linear trend + Signal 1 + Signal 2 + Signal 3	0.81***	0.76***	0.56***	0.63***

[a] The Linear trend in the c47 water yield data was not significant, so subsequent analysis does not include the linear trend
[b] The complete peak for Step 4 in c50 fell outside the window of investigation (i.e. included a scale with a period of more than 14 years), and all other scales had already been included in previous steps (see Table IIID), so this step was not performed.

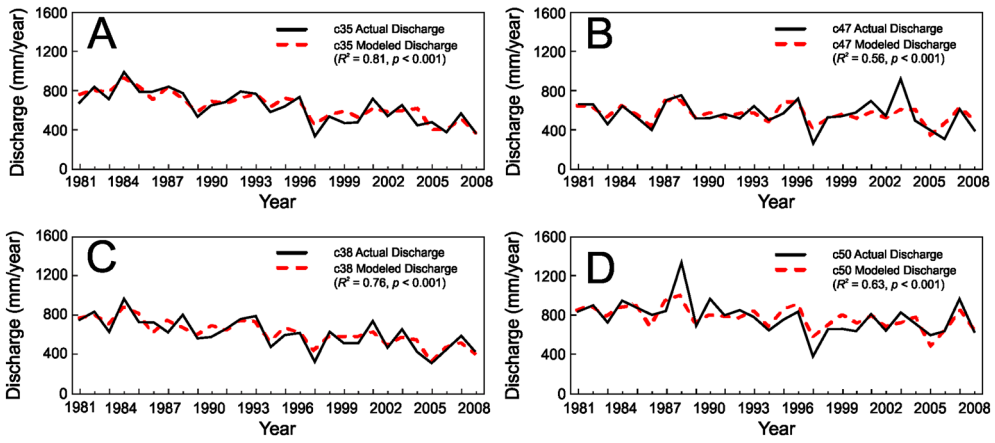

Figure 11. Time series for the observed and modelled yearly water yields over the study time period for the catchments (A) c35, (B) c47, (C) c38, and (D) c50

reflecting the buffering capacity of storage capacity on water discharge fluctuations associated with shorter term periods but not longer term periods.

Our study indicates that drier (lower water loading) catchments with minimal water storage capacity may be better sentinels of climate change in humid regions. The catchment with the lower water loading and lower water storage capacity (c35) was the most sensitive to the non-stationary signal (decline in water yield of −14.6 mm/year) and was the catchment for which we were able to explain the most variation (81%) in water yields through a combination of the non-stationary and stationary signals. In contrast, the catchment with higher water loading and lower water storage capacity (c47) was the least sensitive to the non-stationary signal (no significant decline in water yields), and only 56% of the variation in water yields could be explained through a combination of non-stationary and stationary signals. It is difficult to compare our findings with similar studies in the region or elsewhere because there are few studies that investigate the effect of catchment water loading on climate change related water yield responses. Nonetheless, our study clearly shows that the climatic characteristics of a region within which a catchment is located must be considered prior to selecting the best sentinel for climate change.

Global drivers of local responses in water yields

In the last few decades, scientists have recognized the effects of global climate oscillations on regional climate, particularly on the inter-annual variability of temperature and precipitation in regions thousands of kilometers away from the sites of the initial fluctuations (Ropelewski and Halpert, 1996; Shabbar *et al.*, 1997; Ionita *et al.*, 2012; Zhou *et al.*, 2012). Furthermore, the effects of global climate oscillations on hydrology and associated hydroecological processes of water bodies are well documented (Foley *et al.*, 2002; Kawahata and Gupta, 2003; Kondrashov *et al.*, 2005; Labat, 2008; Keener *et al.*, 2010). We contributed to this body of knowledge by exploring the effects of global climate oscillations on headwater catchment water yields with a local watershed.

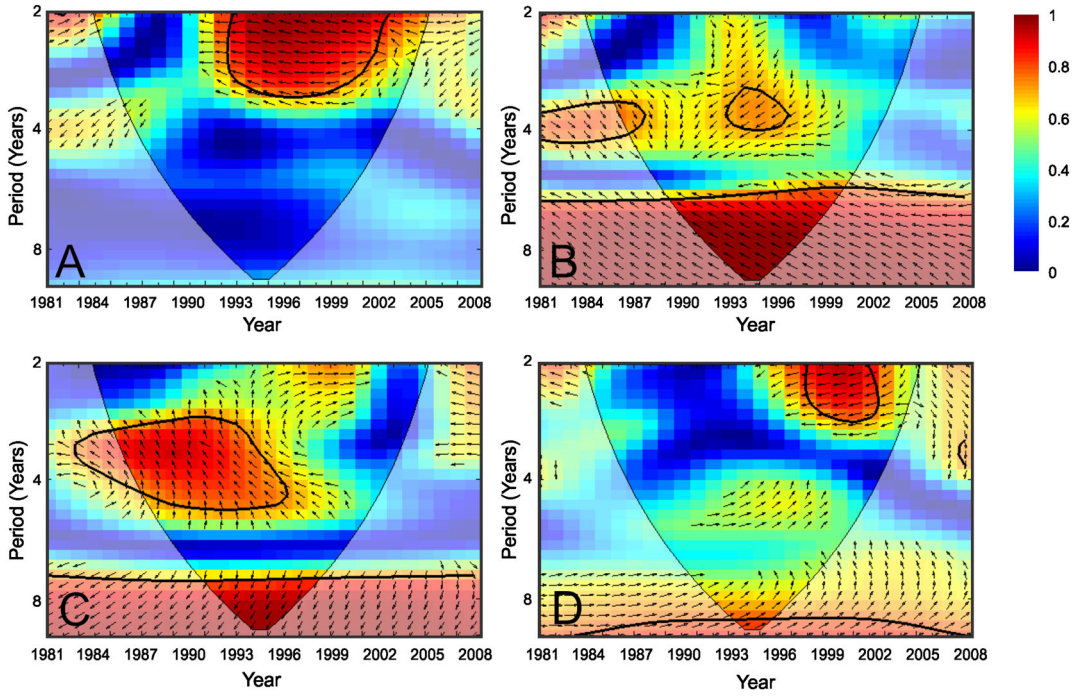

Figure 12. Cross coherence plots using Morlet mother wavelets to generate wavelet power spectra [from Equation (11)] show correlations at each period between yearly water yield of c35 and (A) MEI, (B) AMO, (C) NAO, and (D) PDO. The thin solid line represents the cone of influence, the thick contours indicate the 95% significance level, arrows show the relative phase relationship (left arrows for negative correlations and right arrows for positive correlations). Warm colours indicate strong correlations and cool colours indicate weak relationships along a linear scale

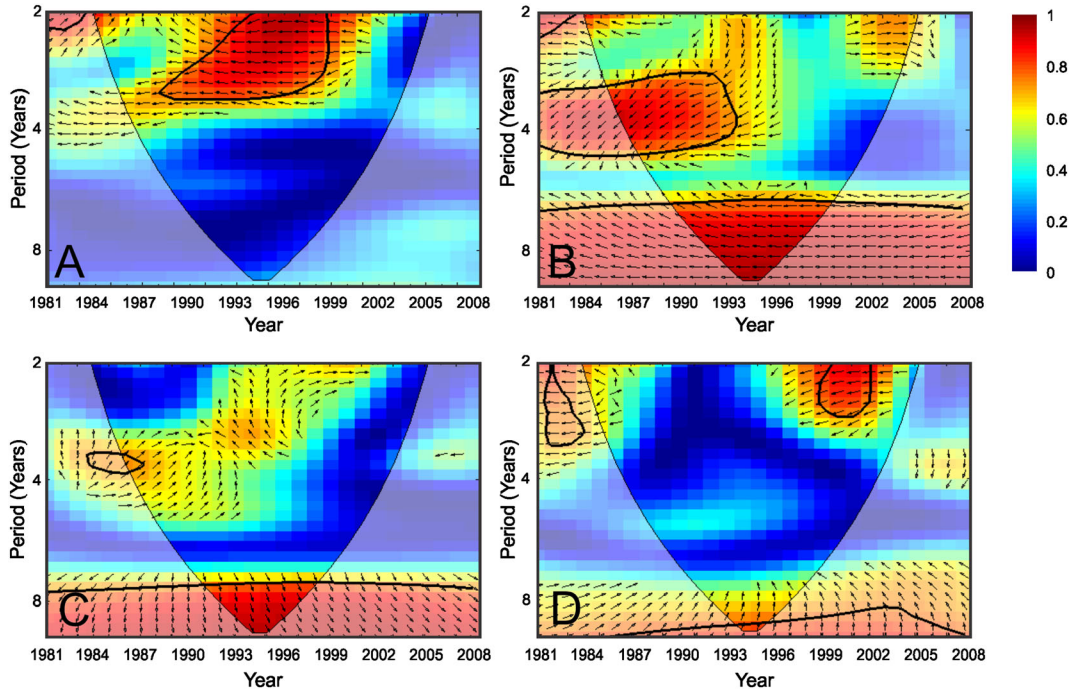

Figure 13. Cross coherence plots using Morlet mother wavelets to generate wavelet power spectra [from Equation (11)] show correlations at each period between yearly water yield of c38 and (A) MEI, (B) AMO, (C) NAO, and (D) PDO. The thin solid line represents the cone of influence, the thick contours indicate the 95% significance level, arrows show the relative phase relationship (left arrows for negative correlations and right arrows for positive correlations). Warm colours indicate strong correlations and cool colours indicate weak relationships along a linear scale

The non-stationary trend was linked to climate warming. One of the original assumptions of this research is that at least part of the observed increase in temperature in the TLW (0.067 °C per year, Figure 3) is being caused by anthropogenic climate warming. We were able to show that the AMO index and temperature are significantly correlated both using the TLW data and the longer term data from the Sault Ste. Marie, Michigan weather station over two distinct

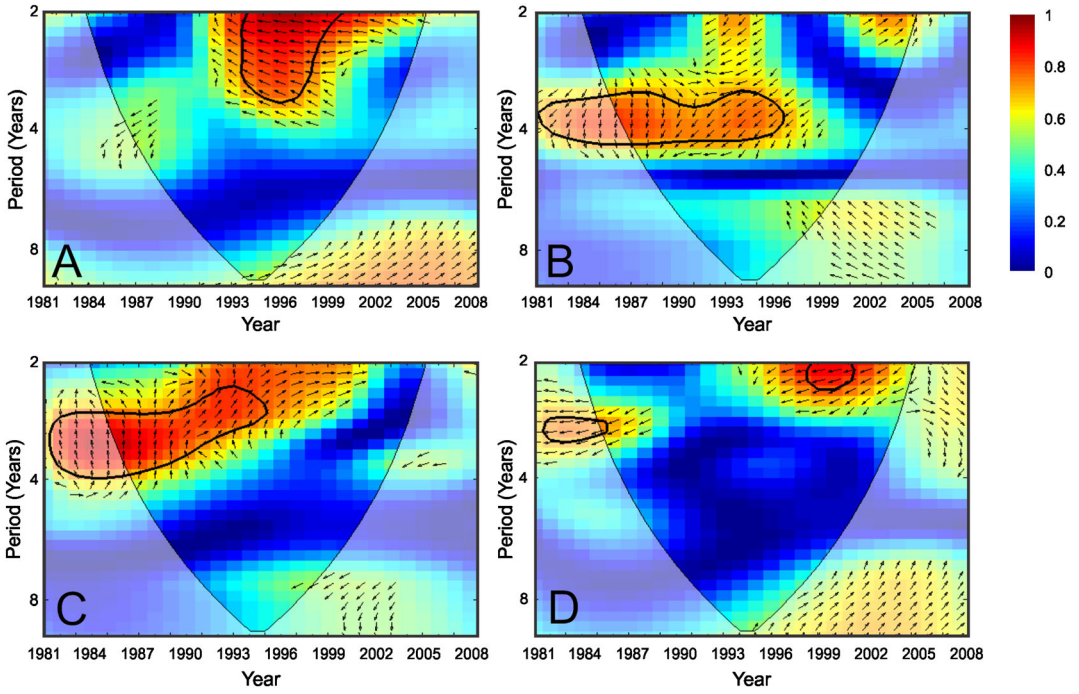

Figure 14. Cross coherence plots using Morlet mother wavelets to generate wavelet power spectra [from Equation (11)] show correlations at each period between yearly water yield of c47 and (A) MEI, (B) AMO, (C) NAO, and (D) PDO. The thin solid line represents the cone of influence, the thick contours indicate the 95% significance level, arrows show the relative phase relationship (left arrows for negative correlations and right arrows for positive correlations). Warm colours indicate strong correlations and cool colours indicate weak relationships along a linear scale

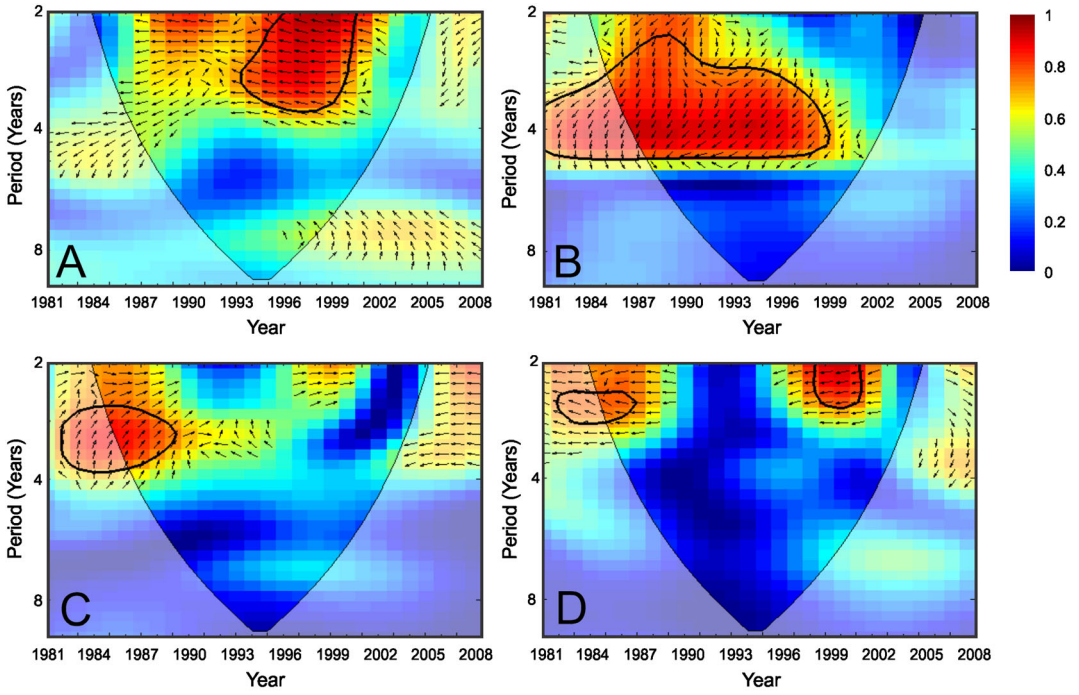

Figure 15. Cross coherence plots using Morlet mother wavelets to generate wavelet power spectra [from Equation (11)] show correlations at each period between yearly water yield of c50 and (A) MEI, (B) AMO, (C) NAO, and (D) PDO. The thin solid line represents the cone of influence, the thick contours indicate the 95% significance level, arrows show the relative phase relationship (left arrows for negative correlations and right arrows for positive correlations). Warm colours indicate strong correlations and cool colours indicate weak relationships along a linear scale

AMO cycles (1901 to 1963 and 1963 to 2010). By using the longer term data, we were able to show that temperature at the minimum AMO values increases by approximately 0.037 °C per year until the maximum AMO values (approximately 30 years). Coincidentally, the TLW data record (1981 to 2008) corresponded with an AMO minimum to maximum half cycle (Figure 6), meaning that the TLW was being affected both by strong non-stationary

Table V. Pearson product moment correlations between the annual average values of Multivariant El Niño Southern Oscillation (ENSO) Index (MEI), Atlantic Multidecadal Oscillation (AMO), Northern Atlantic Oscillation (NAO), and Pacific Decadal Oscillation (PDO) (* indicates $p < 0.05$; *** indicates $p < 0.001$)

	MEI	AMO	NAO	PDO
MEI	–	−0.152	0.011	0.600***
AMO	–	–	−0.387	−0.314
NAO	–	–	–	−0.387*
PDO	–	–	–	–

and stationary signals. We estimate that of the 0.067 °C per year increase in temperature observed from 1981 to 2008, 0.037 °C per year can be explained by the AMO index (from interpolated temperatures of 3.81 °C at the minimum AMO value and 4.96 °C at the maximum value over a 31-year half-cycle, Figure 16A), leaving 0.030 °C for other causes, including anthropogenic climate change. It is possible that some of the increase in temperature ascribed to AMO is also, at least in part, caused by anthropogenic climate change. For example, Guan and Nigam (2009) state that non-stationary trends, such as anthropogenic climate warming, can affect Atlantic Sub-surface Temperature, potentially aliasing effects of global warming into natural climate oscillations.

The stationary trend was linked to global climate oscillations, with the highest frequency (2 to 3.6 years) associated with MEI and PDO, a moderate frequency (3.5 to 6 years) associated with AMO, and the lowest frequency (6.73 to 9.51) associated with NAO. Each of these global climate oscillation indices was correlated to local water yields, but the timing, persistence, and direction of correlations varied. From the complex patterns in the wavelet cross coherence plots (Figures 9–12), the following generalizations were made: (1) The period of high, negative correlations between MEI or PDO and water yields was longer in duration in the lower water loading catchments (c35, c38) compared to higher water loading catchments (c47, c50) – as the MEI or PDO increase, climate is warmer, drier and water yields decrease; (2) The period of high, generally negative correlations between the AMO and water yields was shorter in duration in the lower water loading catchments (c35, c38) compared to higher water loading catchments (c47, c50) – as the AMO increases, the climate gets warmer with less rain and water yields decrease; and (3) The period of high, generally positive correlations between the NAO and water yields was longer in duration in the lower water storage capacity catchments (c35, c47) compared to higher water storage capacity catchments (c38, c50) – as the NAO increases, climate is cooler, wetter and water yields increase. Global climate oscillations have prolonged effects on water yields from catchments with lower water loading (c35, c38) and lower water storage capacity (c35, c47).

Some of the global climate oscillation indices had interactive effects. The positive correlation between the MEI and PDO indicates that as the MEI increases (reflecting warmer, drier conditions) or decreases (reflecting cooler, wetter conditions), the effects on climatic conditions may be amplified by the PDO. The negative correlation between the NAO and PDO indicates that as the NAO index increases (reflecting cooler, wetter conditions) or decreases (reflecting warmer, drier conditions), the effects on climatic conditions may be amplified by the PDO (Table V).

Future consideration of finer time series of water yield data

This study used yearly time series of water yields rather than finer time scales. In our data analysis, the residuals (observed data minus trend) are consistent with white noise, but there may be additional features that this type of data cannot detect, for example persistent wetness levels over a period of a few months. Future work using finer time scales may reveal if there is a stochastic persistence such as autoregressive time series dependence in the noise, or if there is coherence with respect to other climate oscillation indices such as NOA or PDO on this finer scale. The cross coherence analysis shows there is some correlation or dependence between the catchment data and the global climate oscillation indices. In future studies that focus on intra-annual data, we will explore if there is lag dependence between the catchment data and

Table VI. Correlations between climatic indices and the identified stationary signals for four catchments in the Turkey Lakes Watershed demonstrating the indices that are the most strongly correlated

Catchment	Stationary signal	Periods (years)	Strongest correlated index	R^2 (Direction of correlation)	p
c35	1	6.73 to 9.51	PDO	0.220 (+)	**0.013**
	2	2 to 2.83	MEI	0.026 (-)	0.414
	3	3.36 to 4.76	MEI	0.150 (-)	**0.039**
c38	1	2 to 2.83	NAO	0.010 (-)	0.619
	2	6.73 to 9.51	AMO	0.250 (-)	**0.007**
	3	3.36 to 4.76	MEI	0.240 (-)	**0.009**
c47	1	6.73 to 9.51	NAO	0.009 (-)	0.636
	2	2 to 2.83	MEI	0.014 (-)	0.552
	3	3.36 to 4.76	MEI	0.210 (-)	**0.015**
c50	1	2 to 2.83	MEI	0.012 (-)	0.575
	2	3.36 to 4.76	MEI	0.210 (-)	**0.014**
	3	5.66 to 8	PDO	0.054 (-)	0.232

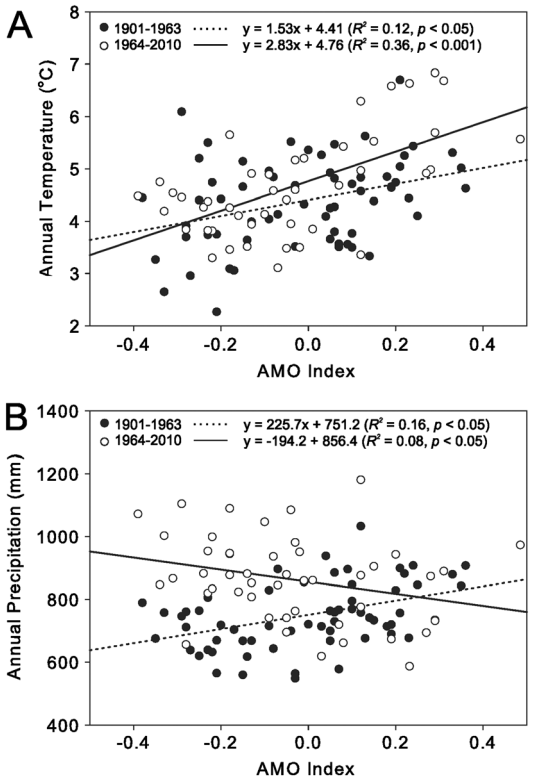

Figure 16. Regressions between the AMO Index and the mean annual precipitation (A) and temperature values (B) from the Sault Ste. Marie, Michigan weather station during two distinct AMO cycles (1901–1964 and 1964–2010)

previous values of these indices. We have not checked the cross coherence of the indices with the residuals due to the length of the time series and the fact that the residuals are consistent with white noise. This additional step would be interesting to see if the regression mean estimates account for the influence of the climate oscillation indices, or if there is further dependence.

Critical need for long-term monitoring recordsA limitation of the presented analyses (and similar analyses in other studies) is the short length of the available data time series. The TLW has one of the longest monitoring records in Canada (Creed *et al*., 2011); even so, it does not allow for full consideration of some of the multi-decadal global climate oscillations. For example, the MEI has a 2- to 7-year cycle (Huggett, 1997); NAO has no statistically significant periodicity, although there is some evidence of a 7- to 9-year and approximately a 20-year cycle (Burroughs, 2005); PDO has a 20- to 30-year cycle (Burn, 2008); and AMO has a 60- to 90-year cycle (Knudsen *et al*., 2011). Complete cycles for MEI and NAO only would be captured in the 28-year record for the TLW. A potential danger of this short time series is that the apparent non-stationary signal may exaggerate the stated influence of climate warming. Even still, with an observation window that included only half of the AMO cycle, we were able to observe significant correlations between climate and the AMO index and to ascribe more than half the non-stationary temperature increase in the TLW to this relationship. Continued support and investment in long-term catchment studies, and analysis of social factors that influence water supply and demand, will help civic institutions adapt to future scenarios of climate and land-use change (Creed *et al*., 2011; Jones *et al*., 2012).

CONCLUSIONS

Climatic change has complex influences on headwater catchment water yields. To determine effects of climate change, we must be able to discriminate between anthropogenic climate warming (non-stationary trends) and natural climate oscillation (stationary cycles) signals on catchment water yields from catchments. Using our analytical framework, we were able to show that: (1) headwater catchments showed a general non-stationary decline in water yields, which may have been caused by the 1 degree Celsius per decade climate warming that has occurred within the region; however, individual catchments varied in their responsiveness to climate change, with catchments that have lower water loading and lower water storage capacity being the most sensitive; (2) headwater catchments showed stationary cycles in water yields caused by specific climate oscillations or possibly the interactive impacts of multiple global climate oscillations, which are sometimes significantly correlated with each other; and (3) by combining the models of stationary and non-stationary signals identified, it was possible to explain the majority of the variance in water yields within each catchment. AMO was identified as the index most closely associated with climate in the TLW, and it explained approximately 0.037 °C of the observed 0.067 °C per year increase in temperature from 1981 to 2008. The methodology developed in this study can be used not only to understand hydrologic responses to climate change, but also associated biogeochemical responses, including carbon, nitrogen, and phosphorus export. Future work will extend the analytical framework to include seasonal, monthly, and daily data as well as predicting both water and solute yields from headwater catchments within the TLW and will apply this methodology to other catchments from long-term monitoring stations with the longest available records in forested landscapes across northern latitudes in North America.

ACKNOWLEDGEMENTS

This research was funded by a Natural Sciences and Engineering Research Council of Canada Discovery Grant to IFC (217053-2009 RGPIN) and RJK (5724-2011 RGPIN). The TLW is managed by several federal government agencies, and we acknowledge contributions by F. Beall, J. Nicolson (Natural Resources Canda, Canadian Forest Service), R. Semkin, D. Jeffries (Environment Canada, National Water Research Institute), and R. Vet (Environment Canada, Meteorological Service of Canada) to the TLW database that was used in this study. We

acknowledge Mr. Johnston Miller for his assistance with editing the manuscript and preparing the graphics. We thank two anonymous reviewers for providing insightful comments that improved the manuscript.

REFERENCES

Arnell N. 2004. Climate change and global water resources: SRES emissions and socio-economic scenarios. *Global Environmental Change-Human and Policy Dimensions* **14**: 31–52. DOI: 10.1016/j.goenvcha.2003.10.006

Bishop K, Buffam I, Erlandsson M, Folster J, Laudon H, Seibert J, Temnerud J. 2008. Aqua Incognita: the unknown headwaters. *Hydrological Processes* **22**: 1239–1242. DOI: 10.1002/hyp.7049

Bonsal B, Shabbar A, Higuchi K. 2001. Impacts of low frequency variability modes on Canadian winter temperature. *International Journal of Climatology* **21**: 95–108. DOI: 10.1002/joc.590

Burn DH. 2008. Climatic influences on streamflow timing in the headwaters of the Mackenzie River Basin. *Journal of Hydrology* **352**: 225–238. DOI: 10.1016/j.jhydrol.2008.01.019

Burroughs WJ. 2005. Cycles and periodicities. In *Encyclopedia of World Climatology*, Oliver JE (ed). Springer-Dordrecht: The Netherlands; 173–177.

Canada Soil Survey Committee. 1978. Canadian system of soil classification. Publ. 1646, 164 pp., Dep. of Agri., Ottawa.

Carey SK, Tetzlaff D, Seibert J, Soulsby C, Buttle J, Laudon H, McDonnell J, McGuire K, Caissie D, Shanley J, Kennedy M, Devito K, Pomeroy JW. 2010. Inter-comparison of hydro-climatic regimes across northern catchments: synchronicity, resistance and resilience. *Hydrological Processes* **24**: 3591–3602. DOI: 10.1002/hyp.7880

Chen Y, Takeuchi K, Xu C, Chen Y, Xu Z. 2006. Regional climate change and its effects on river runoff in the Tarim Basin, China. *Hydrological Processes* **20**: 2207–2216. DOI: 10.1002/hyp.6200

Christensen NS, Wood AW, Voisin N, Lettenmaier DP, Palmer RN. 2004. The effects of climate change on the hydrology and water resources of the Colorado River basin. *Climatic Change* **62**: 337–363. DOI: 10.1023/B:CLIM.0000013684.13621.1f

Clarke A, Mac Nally R, Bond N, Lake PS. 2008. Macroinvertebrate diversity in headwater streams: a review. *Freshwater Biology* **53**: 1707–1721. DOI: 10.1111/j.1365-2427.2008.02041.x

Cowell DW, Wickware GM. 1983. Preliminary analyses of soil chemical and physical properties, Turkey Lakes Watershed, Algoma, Ontario. Rep. 83-08, Turkey Lakes Watershed, Algoma, Ontario, Canada.

Creed IF, Sanford SE, Beall FD, Molot LA, Dillon PJ. 2003. Cryptic wetlands: integrating hidden wetlands in regression models of the export of dissolved organic carbon from forested landscapes. *Hydrological Processes* **17**: 3629–3648. DOI: 10.1002/hyp.1357

Creed IF, Beall FD, Clair TA, Dillon PJ, Hesslein RH. 2008. Predicting export of dissolved organic carbon from forested catchments in glaciated landscapes with shallow soils. *Global Biogeochemical Cycles* **22**: GB4024. DOI: 10.1029/2008GB003294

Creed IF, Sass GZ, Beall FD, Buttle JM, Moore RD, Donnelly M. 2011. Scientific theory, data and techniques for conservation of water resources within a changing forested landscape. A State of Knowledge report. Sustainable Forest Management Network, Edmonton, Alberta, 136.

Eimers M, Dillon P, Watmough S. 2004. Long-term (18-year) changes in sulphate concentrations in two Ontario headwater lakes and their inflows in response to decreasing deposition and climate variations. *Hydrological Processes* **18**: 2617–2630. DOI: 10.1002/hyp.5570

Elliot H. 1985. Geophysical survey to determine overburden thickness in selected areas within the Turkey Lakes Watershed basin, Algoma District, Ontario. Rep. 85-09, Turkey Lakes Watershed, Algoma, Ontario, Canada.

Farge M. 1992. Wavelet transforms and their applications to turbulence. *Annual Review of Fluid Mechanics* **24**: 395–457. DOI: 10.1146/annurev.fluid.24.1.395

Feminella J. 1996. Comparison of benthic macroinvertebrate assemblages in small streams along a gradient of flow permanence. *Journal of the North American Benthological Society* **15**: 651–669. DOI: 10.2307/1467814

Foley J, Botta A, Coe M, Costa M. 2002. El Nino-Southern Oscillation and the climate, ecosystems and rivers of Amazonia RID A-5695-2009. *Global Biogeochemical Cycles* **16**: 1132. DOI: 10.1029/2002GB001872

Gaucherel C. 2010. Analysis of ENSO interannual oscillations using non-stationary quasi-periodic statistics: a study of ENSO memory. *International Journal of Climatology* **30**: 926–934. DOI: 10.1002/joc.1937

Giblin PE, Leahy EJ. 1977. Geological compilation of the Batchawana sheet, Districts of Algoma and Sudbury, Ontario. Preliminary Map 302, Geol. Surv. Can., Ontario.

Gomi T, Sidle R, Richardson J. 2002. Understanding processes and downstream linkages of headwater systems RID E-3504-2010. *Bioscience* **52**: 905–916. DOI: 10.1641/0006-3568(2002)052[0905:UPADLO]2.0.CO;2

Grinsted A, Moore J, Jevrejeva S. 2002. Cross wavelet and wavelet coherence Matlab Package. Downloaded from http://www.pol.ac.uk/home/research/waveletcoherence/ on October 15, 2011.

Grinsted A, Moore J, Jevrejeva S. 2004. Application of the cross wavelet transform and wavelet coherence to geophysical time series. *Nonlinear Processes in Geophysics* **11**: 561–566.

Guan B, Nigam S. 2009. Analysis of Atlantic SST variability factoring interbasin links and the secular trend: Clarified structure of the Atlantic Multidecadal Oscillation. *Journal of Climate* **22**: 4228–4240. DOI: 10.1175/2009JCLI2921.1

Haycock NE, Pinay G, Walker C. 1993. Nitrogen-Retention in River Corridors - European Perspective. *Ambio* **22**: 340–346.

Huggett RJ. 1997. *Environmental change. The evolving ecosphere*. Routledge: London; 119.

Ionita M, Lohmann G, Rimbu N, Chelcea S, Dima M. 2012. Interannual to decadal summer drought variability over Europe and its relationship to global sea surface temperature. *Climate Dynamics* **38**: 363–77. DOI: 10.1007/s00382-011-1028-y

Jeffries DS, Semkin RS. 1982. Basin description and information pertinent to mass balance studies of the Turkey Lakes Watershed. Rep. 82-01, Turkey Lakes Watershed, Algoma, Ontario, Canada.

Jeffries D, Kelso J, Morrison I. 1988. Physical, Chemical, and Biological Characteristics of the Turkey Lakes Watershed, Central Ontario, Canada. *Canadian Journal of Fisheries and Aquatic Sciences* **45**: 3–13.

Joint Institute for the Study of the Atmosphere and Ocean (JISAO). 2012. Pacific Decadal Oscillation (PDO) data. Accessed from http://jisao.washington.edu/pdo/PDO.latest on April 10, 2012.

Jones JA, Creed IF, Hatcher KL, Warren RJ, Adams MB, Benson MH, Boose E, Brown WA, Campbell JL, Covich A, Clow DW, Clifford CN, Elder K, Ford CR, Grimm NB, Henshaw DL, Larson KL, Miles ES, Miles KM, Sebestyen S, Spargo AT, Stone AT, Vose JM, Williams MW. 2012. Ecosystem Processes and Human Influences Regulate Streamflow Response to Climate Change at Long-Term Ecological Research Sites. *BioScience* **62**: 390–404.

Kahya E. 2011. The Impacts of NAO on the Hydrology of the Eastern Mediterranean. *Hydrological, Socioeconomic and Ecological Impacts of the North Atlantic Oscillation in the Mediterranean Region* **46**: 57–71. DOI: 10.1007/978-94-007-1372-7_5

Kang S, Lin H. 2007. Wavelet analysis of hydrological and water quality signals in an agricultural watershed. *Journal of Hydrology* **338**: 1–14. DOI: 10.1016/j.jhydrol.2007.01.047

Kawahata H, Gupta L. 2003. El Nino Southern Oscillation (ENSO) related variations in particulate export fluxes in the western and central equatorial Pacific. *Journal of Oceanography* **59**: 663–670. DOI: 10.1023/B:JOCE.0000009595.79408.13

Keener VW, Feyereisen GW, Lall U, Jones JW, Bosch DD, Lowrance R. 2010. El-Nino/Southern Oscillation (ENSO) influences on monthly NO (3) load and concentration, stream flow and precipitation in the Little River Watershed, Tifton, Georgia (GA). *Journal of Hydrology* **381**: 352–363. DOI: 10.1016/j.jhydrol.2009.12.008

Kirby MJ. 1978. *Hillslope hydrology*. John Wiley and Sons: Chichester, United Kingdom.

Knight JR, Folland CK, Scaife AA. 2006. Climate impacts of the Atlantic Multidecadal Oscillation. *Geophysical Research Letters* **33**: L17706. DOI: 10.1029/2006GL026242

Knudsen MF, Seidenkrantz M, Jacobsen BH, Kuijpers A. 2011. Tracking the Atlantic Multidecadal Oscillation through the last 8,000 years RID A-3451-2012 RID A-4854-2012. *Nature Communications* **2**: 178. DOI: 10.1038/ncomms1186

Kondrashov D, Feliks Y, Ghil M. 2005. Oscillatory modes of extended Nile River records (AD 622-1922). *Geophysical Research Letters* **32**: L10702. DOI: 10.1029/2004GL022156

Labat D. 2005. Recent advances in wavelet analyses: Part I. A review of concepts. *Journal of Hydrology* **314**: 275–288. DOI: 10.1016/j.jhydrol.2005.04.003

Labat D. 2008. Wavelet analysis of the annual water yield records of the world's largest rivers. *Advances in Water Resources* **31**: 109–117. DOI: 10.1016/j.advwatres.2007.67.004

Lindsay JB, Creed IF, Beall FD. 2004. Drainage basin morphometrics for depressional landscapes. *Water Resources Research* **40**: W09307. DOI: 10.1029/2004WR003322

Mantua N, Hare S. 2002. The Pacific decadal oscillation. *Journal of Oceanography* **58**: 35–44. DOI: 10.1023/A:1015820616384

Meyer JL, Wallace JB. 2001. Lost linkages and lotic ecology: Rediscovering small streams. In *Ecology: Achievement and Challenge*, Huntly NJ, Levin S (eds). Blackwell Publishing: Oxford; 295–317.

Minobe S. 1997. A 50-70 year climatic oscillation over the North Pacific and North America. *Geophysical Research Letters* **24**: 683–6. DOI: 10.1029/97GL00504

National Center for Atmospheric Research (NCAR). 2012. Northern Atlantic Oscillation (NAO) data. Accessed from https://climatedataguide.ucar.edu/sites/default/files/cas_data_files/asphilli/nao_station_monthly_0.txt on April 10, 2012.

National Oceanic and Atmospheric Administration – Earth System Research Laboratory (NOAA – ESRL). 2012a. Multivariate El Niño Southern Oscillation (ENSO) Index (MEI) data. Accessed from http://www.esrl.noaa.gov/psd/enso/mei/table.html on April 10, 2012.

National Oceanic and Atmospheric Administration – Earth System Research Laboratory (NOAA – ESRL). 2012b. Atlantic Multidecadal Oscillation (AMO) data. Accessed from http://www.esrl.noaa.gov/psd/data/correlation/amon.us.long.data on April 10, 2012.

Nicolson JA. 1988. Water and chemical budgets for terrestrial basins at the Turkey Lakes Watershed. *Canadian Journal of Fisheries and Aquatic Sciences* **45**: 88–95.

Niedzielski T. 2011. Is there any teleconnection between surface hydrology in Poland and El Nino/Southern Oscillation? *Pure and Applied Geophysics* **168**: 871–886. DOI: 10.1007/s00024-010-0171-4

Pike RG, Spittlehouse DL, Bennett KE, Egginton VN, Tschaplinski PJ, Murdock TQ, Werner AT. 2008. Climate Change and Watershed Hydrology: Part I - Recent and Projected Changes in British Columbia. *Streamline Watershed Management Bulletin* **11**: 1–7.

Price DT, McKenney DW, Joyce LA, Siltanen RM, Papadopol P, Lawrence K. 2011. High-resolution interpolation of climate scenarios for Canada derived from General Circulation Model Simulations. Natural Resources Canada Information Report NOR-X-421.

Rabeni C, Wallace G. 1998. The influence of flow variation on the ability to evaluate the biological health of headwater streams. In *Hydrology, Water Resources and Ecology in Headwaters*, Kovar K, Tappeiner U, Peters NE, Craig RG (eds). IAHS: 411–418.

Ropelewski C, Halpert M. 1996. Quantifying Southern Oscillation - Precipitation relationships. *Journal of Climate* **9**: 1043–1059. DOI: 10.1175/1520-0442(1996)009 < 1043:QSOPR > 2.0.CO;2

Santos CAG, De Morais BS. 2008. Hydrological zones of San Francisco river basin by wavelet transform. In *Proceedings of HydroPredict 2008*, Bruthans J, Kovar K, Hrkal Z (eds). Prague, Czech Republic; 1–8.

Semkin RG, Jeffries DS, Neureuther R, Lahaie G, Norouzian F, Franklyn J. 2001. Summary of hydrological and meteorological measurements in the Turkey Lakes Watershed, Algoma, Ontario, 1980–1999 National Water Research Institute, Environment Canada, Burlington, Ontario.

Shabbar A, Bonsal B. 2004. Associations between low frequency variability modes and winter temperature extremes in Canada. *Atmosphere-Ocean* **42**: 127–140. DOI: 10.3137/ao.420204

Shabbar A, Khandekar M. 1996. The impact of El Nino-Southern Oscillation on the temperature field over Canada. *Atmosphere-Ocean* **34**: 401–416.

Shabbar A, Bonsal B, Khandekar M. 1997. Canadian precipitation patterns associated with the southern oscillation. *Journal of Climate* **10**: 3016–3027. DOI: 10.1175/1520-0442(1997)010 < 3016:CPPAWT > 2.0.CO;2

Sidle R, Tsuboyama Y, Noguchi S, Hosoda I, Fujieda M, Shimizu T. 2000. Stormflow generation in steep forested headwaters: a linked hydrogeomorphic paradigm. *Hydrological Processes* **14**: 369–385. DOI: 10.1002/(SICI)1099-1085(20000228)14:3 < 369::AID-HYP943 3.0.CO;2-P

Soniat TM, Klinck JM, Powell EN, Hofmann EE. 2006. Understanding the success and failure of oyster populations: Climatic cycles and Perkinsus marinus. *Journal of Shellfish Research* **25**: 83–93. DOI: 10.2983/0730-8000(2006)25[83:UTSAFO]2.0.CO;2

Strand LT, Haaland S, Kaste O, Stuanes AO. 2008. Natural variability in soil and runoff from small headwater catchments at Storgama, Norway. *Ambio* **37**: 18–28. DOI: 10.1579/0044-7447(2008)37[18:NVISAR]2.0.CO;2

Torrence C, Compo G. 1998. A practical guide to wavelet analysis. *Bulletin of the American Meteorological Society* **79**: 61–78. DOI: 10.1175/1520-0477(1998)079 < 0061:APGTWA > 2.0.CO;2

Torrence C, Webster P. 1999. Interdecadal changes in the ENSO-monsoon system. *Journal of Climate* **12**: 2679–2690. DOI: 10.1175/1520-0442(1999)012 < 2679:ICITEM > 2.0.CO;2

Wickware GM, Cowell DW. 1985. Forest Ecosystem Classification of the Turkey Lake Watershed, Ecol. Classif. Ser. 18, Lands Dir., Environ, Ottawa, Canada.

Winter TC. 2000. The vulnerability of wetlands to climate change: A hydrologic landscape perspective. *Journal of the American Water Resources Association* **36**: 305–11. DOI: 10.1111/j.1752-1688.2000.tb04269.x

Wipfli M, Gregovich D. 2002. Export of invertebrates and detritus from fishless headwater streams in southeastern Alaska: implications for downstream salmonid production. *Freshwater Biology* **47**: 957–69. DOI: 10.1046/j.1365-2427.2002.00826.x

Zhou T, Zhang L, Li H. 2008. Changes in global land monsoon area and total rainfall accumulation over the last half century. *Geophysical Research Letters* **35**: L16707. DOI: 10.1029/2008GL034881

Zhou W, Chen W, Wang DX. 2012. The implications of El Niño-Southern Oscillation signal for South China monsoon climate. *Aquatic Ecosystem Health & Management* **15**: 14–19.

Zwiers FW, Schnorbus MA, Maruszeczka GD. 2011. Hydrologic impacts of climate change on BC water resources. Summary report for Campbell, Columbia and Peace River watersheds. Pacific Climate Impacts Consortium: University of Victoria, Victoria, BC.

